

## Experimental implementation of a fully controllable depolarizing quantum operation

Youn-Chang Jeong, Jong-Chan Lee, and Yoon-Ho Kim

*Department of Physics, Pohang University of Science and Technology (POSTECH), Pohang 790-784, Korea*

(Received 23 October 2012; published 14 January 2013)

The depolarizing quantum operation plays an important role in studying the quantum noise effect and implementing general quantum operations. In this work, we report a scheme which implements a fully controllable input-state-independent depolarizing quantum operation for a photonic polarization qubit.

DOI: [10.1103/PhysRevA.87.014301](https://doi.org/10.1103/PhysRevA.87.014301)

PACS number(s): 03.67.Hk, 03.65.Yz, 42.50.Ex, 42.50.Lc

One of the main challenges in experimental quantum information is to deal with decoherence. To preserve a qubit state, it is often necessary to isolate the qubit from the environment but to be able to do information-processing tasks, interactions with external systems are necessary. More often than not, unwanted interactions with the environment leave the system qubits in different quantum states or even cause the qubits to lose coherence. Such unwanted quantum state transformation can be described by the quantum process due to a noisy quantum channel, in other words, a noisy quantum process, which can be understood with a few basic single-qubit noise operations including the bit-flip, the phase-flip, depolarization, and amplitude damping [1].

Understanding and being able to implement each of the basic quantum noise processes are important in theoretical and experimental quantum-information science. First, this would allow us to simulate and quantify quantum noise processes. Second, the bit-flip and the phase-flip operations are essential for quantum error-correction protocols. Third, the depolarization and the amplitude damping operations can describe decoherence.

The depolarization operation is of particular interest because, in addition to being relevant to a number of practical quantum communication and computation scenarios [2–7], it is also an essential operation for optimally approximating nonphysical quantum operations [8,9] and for generating exotic quantum states including Werner states [10] and bound entangled states [11]. Clearly, from the experimental point of view, it is important to develop a method to achieve a fully controllable input-independent depolarization quantum operation.

As such, there have been many reports on experimental implementation of a depolarization quantum channel. In Ref. [12], optical scattering media were used to achieve the depolarization quantum channel but the scheme naturally induces the spread in the photon momenta and it is difficult to control the degree of depolarization in that scheme. Controllable depolarization channels were demonstrated in Refs. [13,14] but the output state was dependent on the input state. An input-independent depolarizing quantum operation was demonstrated in Refs. [3,4,15] by time averaging of many “fast” operations, i.e., an incoherent sum of many different pure quantum states. Continuously variable depolarization was demonstrated in Ref. [16], but that scheme relied on tracing out of the time degree of freedom, and using a reversed set of crystals could in fact reverse the effect of the channel.

In this Brief Report, we report an experimental implementation of a fully controllable depolarization quantum operation for a photonic polarization qubit. The scheme is completely input-state independent so that it is possible to introduce any desired degree of depolarization regardless of the state of the input qubit. Furthermore, our scheme does not rely on time averaging or spatial averaging so that neither the measurement duration nor the measurement affect the output quantum state. In other words, our scheme achieves a truly observer-independent depolarizing quantum operation.

The depolarizing quantum operation is described as

$$\mathcal{E}(\rho) = \frac{pI}{2} + (1-p)\rho, \quad (1)$$

where  $p$  is the degree of decoherence ( $0 \leq p \leq 1$ ),  $\rho$  is the input state of the photonic polarization qubit, and  $I$  is the two-dimensional identity matrix. It can be also written in the operator sum representation as  $\mathcal{E}(\rho) = (1 - \frac{3p}{4})I\rho I + \frac{p}{4}(X\rho X + Y\rho Y + Z\rho Z)$ , where  $X$ ,  $Y$ , and  $Z$  are Pauli operators. Note that the depolarizing quantum operation is nonunitary so it should not be possible to reverse it linearly.

We implement the depolarizing operation  $\mathcal{E}(\rho)$  by using a modified displaced Sagnac interferometer setup as shown in Fig. 1. The displaced Sagnac interferometer [17] consists of a polarizing beam splitter (PBS) and two half-wave plates that can be oriented at the angle  $\theta$  (@ $\theta$  in Fig. 1). Another half-wave plate fixed at  $45^\circ$  at the output mode  $B$  makes the polarization state of the two output modes  $A$  and  $B$  identical.

It is not difficult to see that the displaced Sagnac interferometer in Fig. 1 acts as a continuously variable nonpolarizing beam splitter in which the output ratio  $A : B = 1 - p : p$  can be linearly varied by setting the angle  $\theta$  of the two half-wave plates. Note that the splitting parameter  $p = \sin^2(2\theta)$ . This is confirmed in the experiment as shown in Fig. 2. In the experiment, we prepared the single-photon polarization qubit  $\rho$  by using the heralded single-photon state generated from spontaneous parametric down-conversion (SPDC) in a 3-mm type-II  $\beta$ -barium borate crystal. The wavelength of the pump and that of the SPDC photon, respectively, are 405 and 810 nm. The input polarization qubit was prepared in a pure state  $\rho = |\psi\rangle\langle\psi|$  by using a half-wave plate and a quarter-wave plate. We then measured the count rates at the two single-photon detectors placed at the output ports  $A$  and  $B$  and the data are shown in Fig. 2. As expected, the data show the linear splitting ratio between the two outputs  $A$  and  $B$  with the splitting parameter  $p$ . In Fig. 2, we plot the averaged normalized outputs  $A$  and  $B$  for six input polarization states:  $|H\rangle$  (horizontal),  $|V\rangle$

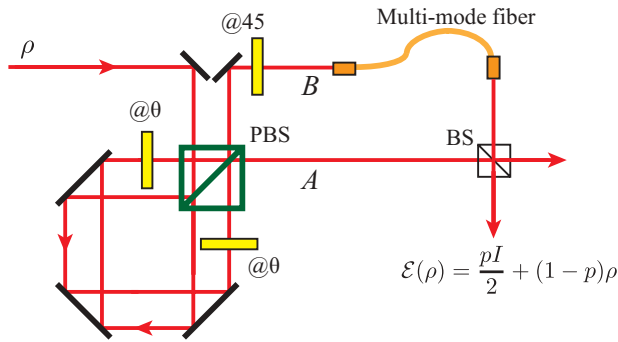


FIG. 1. (Color online) Experimental schematic for a fully controllable input-independent depolarizing quantum operation for a photonic polarization qubit  $\rho$ .

(vertical),  $|D\rangle \equiv (|H\rangle + |V\rangle)/\sqrt{2}$ ,  $|A\rangle \equiv (|H\rangle - |V\rangle)/\sqrt{2}$ ,  $|R\rangle \equiv (|H\rangle - i|V\rangle)/\sqrt{2}$ , and  $|L\rangle \equiv (|H\rangle + i|V\rangle)/\sqrt{2}$ . The normalized outputs  $A$  and  $B$  for each polarization state look almost identical to the averaged result shown in Fig. 2. We also point out that the linearity and the splitting ratio are very stable over time due to the Sagnac geometry.

Previously reported continuously variable nonpolarizing beam splitter schemes using a prism pair [18], a sapphire disk [19], and a phase grating [20] were all input-polarization dependent. Note that it was proposed in Ref. [21] that any unitary operation can be implemented using bulk optics; although, since the scheme is based on Mach-Zehnder interferometers, it is inherently unstable. A particular version (50:50 nonvariable beam splitter) of Ref. [21] has been implemented in Ref. [22]. In this work, the continuously variable nonpolarizing beam splitter scheme is based on the displaced Sagnac interferometer and thus is completely input-polarization independent as demonstrated in Fig. 2. Furthermore, the use of the Sagnac interferometer ensures long-term stability without active feedback locking.

To be sure that the displaced Sagnac splits the input probability amplitude into two spatial modes  $A$  and  $B$  without affecting the quantum state  $\rho$ , we have also performed the quantum state tomography of the input qubit as well as the

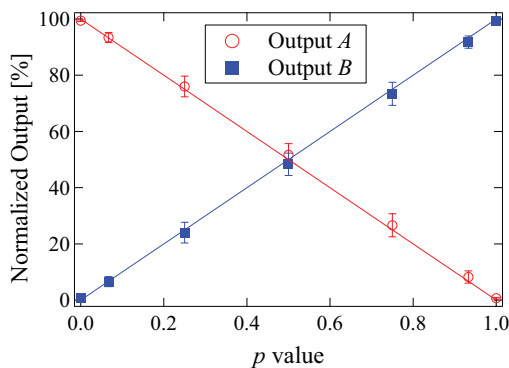


FIG. 2. (Color online) Data showing continuously variable output ratio  $A : B = 1 - p : p$ , where  $p = \sin^2(2\theta)$  for the displaced Sagnac interferometer. Each data point represents the averaged normalized output of six input polarization states:  $|H\rangle$ ,  $|V\rangle$ ,  $|D\rangle$ ,  $|A\rangle$ ,  $|R\rangle$ , and  $|L\rangle$ . The normalized output of each polarization state appears almost identical to the averaged result shown here.

output qubit in modes  $A$  and  $B$  [23]. We observed that the fidelity between the input and the output quantum states is better than  $0.982 \pm 0.003$  for all the polarization qubit states we tested. Thus, the displaced Sagnac acts as a nearly ideal identity operation for the polarization qubit except that it diverts the amplitude into two different spatial modes:  $A$  and  $B$ .

Equation (1) clearly states that to implement the depolarizing quantum operation  $\mathcal{E}(\rho)$  it is necessary to achieve a mixture of the input quantum state  $\rho$  and the unpolarized state  $I/2$  with the weighting factors  $1 - p$  and  $p$ , respectively. Note now that the qubit states found at the outputs  $A$  and  $B$  are identical to the input  $\rho$  but with the probability amplitudes  $1 - p$  and  $p$ , respectively. Thus, we first couple the output mode  $B$  into a 2-m-long multimode fiber to transform a polarized input to a completely unpolarized state. Here the depolarization effect occurs due to intermodal dispersion and intramodal dispersion in the multimode fiber which cause random cross-coupling among orthogonal polarization modes [24]. Since the cross-coupling is strong in a multimode fiber, only a short piece of multimode fiber is necessary. (We used a 2-m-long multimode fiber as it was available to us at the time of the experiment.) We then combine the output of the multimode fiber (after collimation) and that of  $A$  at a beam splitter (BS). The 2-m-long multimode fiber (M31L02, Thorlabs) ensures that the beam combination at the BS is a completely incoherent process since the path length difference is orders of magnitude larger than the single-photon coherence time, which is on the order of hundreds of femtoseconds. Therefore, the quantum state found at the two outputs of the BS is described precisely as  $pI/2 + (1 - p)\rho$ , indicating that the input state  $\rho$  has gone through the depolarizing quantum operation  $\mathcal{E}(\rho)$  in Eq. (1).

To demonstrate that the outputs of the BS indeed correspond to the quantum state after the depolarizing quantum operation, we performed quantum state tomography on the output states for six different input qubit states. The experimental data are shown in Fig. 3. It is clear that, by increasing  $p$ , the qubit states become more mixed, moving toward the center of the

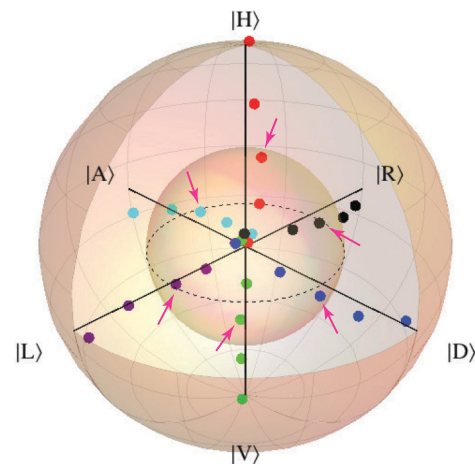


FIG. 3. (Color online) Experimental data. As  $p$  is increased, the qubit states become more mixed and hence move toward the center of the Bloch sphere. The outer sphere represents  $p = 0$  (pure states) and the inner sphere represents  $p = 0.5$ . The arrows point to the data points (i.e., qubit states) on the inner sphere.

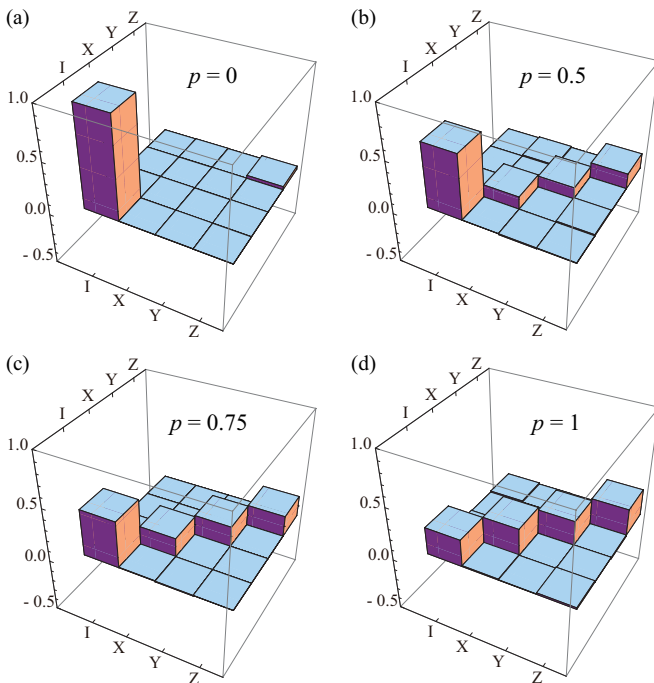


FIG. 4. (Color online) Real part of  $\chi$  matrices of the depolarizing quantum channel.  $I$  refers to the two-dimensional identity matrix.  $X$ ,  $Y$ , and  $Z$  correspond to Pauli operators. The process fidelities (in comparison to the ideal operation) are (a) 0.966, (b) 0.994, (c) 0.998, and (d) 0.997. The imaginary part of the  $\chi$  matrices are almost zero (between  $-0.04$  and  $0.04$  at most) and hence are not shown.

Bloch sphere. Note that changing  $p$  is quite easy in our setup as it requires only the rotation of the wave plates due to the relation  $p = \sin^2(2\theta)$ . It is important to point out that the depolarizing quantum operation is an isotropic operation so that the output state purity  $\text{Tr}[\rho^2]$  does not depend on the input state: it only depends on the choice  $p$ . As such, the depolarizing quantum operation should only shrink the size of the Bloch sphere, rather than making it asymmetric. This feature is well demonstrated in Fig. 3: all the data points corresponding to the depolarizing quantum operation of the same  $p$ , regardless of the input state, should reside on the same sphere. In Fig. 3, the arrows represent the qubit states after the depolarizing quantum operation  $\mathcal{E}(\rho)$  for  $p = 0.5$  and they all lie on the

inner sphere representing all qubit states that have undergone  $\mathcal{E}(\rho)$  with  $p = 0.5$ . Also, Fig. 3 shows that all output states for  $p = 1$  reside at the center of the Bloch sphere, indicating that a 2-m multimode fiber is sufficient to transform a pure polarization state into a completely unpolarized state.

It is known that a quantum channel that implements a particular quantum operation can be fully characterized by performing quantum process tomography [25]. We have carried out quantum process tomography for the depolarizing quantum operation with various  $p$  and the resulting real parts of  $\chi$  matrices are shown in Fig. 4. Clearly, when  $p = 0$ , the quantum process corresponds to an identity operation as it should be [see Fig. 4(a)]. As  $p$  is increased, contributions from the Pauli operations rise [see Figs. 4(b) and 4(c)], and when  $p = 1$ , it is clear that the output state becomes a fully mixed state regardless of the input state [see Fig. 4(d)]. The high process fidelities for various  $p$  values indicate the robustness of our setup to faithfully implement the fully controllable depolarizing quantum operation.

In summary, we have reported an experimental realization of a fully controllable depolarizing quantum operation for a single-photon polarization qubit. Our scheme not only allows continuous adjustment of the degree of depolarization but also the output state is independent of the input quantum state, as demonstrated with quantum state tomography and quantum process tomography. Applications for a versatile depolarizing quantum channel like the one reported in this Brief Report should be found in many areas of photonic quantum-information research, including studying the quantum noise processes [1–6], approximating nonphysical quantum operations [8,9], generating exotic quantum states [10,11], etc. For instance, our scheme can be used to study how the depolarization effect affects the quantum-information processing in an optical system, to generate maximally entangled mixed states involving multiple photonic polarization qubits, to experimentally study the capacity of a quantum communication channel, and to explore the effect of decoherence to multiqubit entangled states [26].

This work was supported in part by the National Research Foundation of Korea (Grants No. 2011-0021452 and No. 2012-002588). J.-C.L. acknowledges support from a National Junior Research Fellowship (Grant No. 2012-000741).

- 
- [1] M. A. Nielsen and I. L. Chuang, *Quantum Computation and Quantum Information* (Cambridge University Press, Cambridge, UK, 2000).
- [2] D. Bruss, L. Faoro, C. Macchiavello, and G. M. Palma, *J. Mod. Opt.* **47**, 325 (2000).
- [3] M. Ricci, F. De Martini, N. J. Cerf, R. Filip, J. Fiurasek, and C. Macchiavello, *Phys. Rev. Lett.* **93**, 170501 (2004).
- [4] A. Chiuri, V. Rosati, G. Vallone, S. Padua, H. Imai, S. Giacomini, C. Macchiavello, and P. Mataloni, *Phys. Rev. Lett.* **107**, 253602 (2011).
- [5] C. M. Dawson, H. L. Haselgrove, and M. A. Nielsen, *Phys. Rev. Lett.* **96**, 020501 (2006).
- [6] C. Cafaro and S. Mancini, *Phys. Rev. A* **82**, 012306 (2010).
- [7] Y. C. Jeong, Y. S. Kim, and Y. H. Kim, *Laser Phys.* **21**, 1438 (2011).
- [8] H. T. Lim, Y. S. Ra, Y. S. Kim, J. Bae, and Y. H. Kim, *Phys. Rev. A* **83**, 020301(R) (2011).
- [9] H. T. Lim, Y. S. Kim, Y. S. Ra, J. Bae, and Y. H. Kim, *Phys. Rev. Lett.* **107**, 160401 (2011).
- [10] M. Barbieri, F. De Martini, G. Di Nepi, and P. Mataloni, *Phys. Rev. Lett.* **92**, 177901 (2004).
- [11] J. Lavoie, R. Kaltenbaek, M. Piani, and K. J. Resch, *Phys. Rev. Lett.* **105**, 130501 (2010).

- [12] G. Puentes, D. Voigt, A. Aiello, and J. P. Woerdman, *Opt. Lett.* **30**, 3216 (2005).
- [13] G. Puentes, D. Voigt, A. Aiello, and J. P. Woerdman, *Opt. Lett.* **31**, 2057 (2006).
- [14] A. Shaham and H. S. Eisenberg, *Phys. Rev. A* **83**, 022303 (2011).
- [15] M. Karpinski, C. Radzewicz, and K. Banaszek, *J. Opt. Soc. Am. B* **25**, 668 (2008).
- [16] A. Shaham and H. S. Eisenberg, *Opt. Lett.* **37**, 2643 (2012).
- [17] M. P. Almeida, F. de Melo, M. Hor-Meyll, A. Salles, S. P. Walborn, P. H. Souto Ribeiro, and L. Davidovich, *Science* **316**, 579 (2007).
- [18] N. J. Harrick, *Appl. Opt.* **2**, 1203 (1963).
- [19] M. M. Broer, C. G. Levey, E. Strauss, and W. M. Yen, *Appl. Opt.* **20**, 1011 (1981).
- [20] Z. Q. Zhong, J. Hua, J. Zhou, and S. H. Wang, *Opt. Commun.* **234**, 7 (2004).
- [21] M. Reck, A. Zeilinger, H. J. Bernstein, and P. Bertani, *Phys. Rev. Lett.* **73**, 58 (1994).
- [22] E. Martin-Zopez, A. Laing, T. Lawson, R. Alvarez, X. Zhou, and J. L. O'Brien, *Nat. Photonics* **6**, 773 (2012).
- [23] D. F. V. James, P. G. Kwiat, W. J. Munro, and A. G. White, *Phys. Rev. A* **64**, 052312 (2001).
- [24] L. Yu and B. S. Rawat, *J. Lightwave Technol.* **10**, 556 (1992).
- [25] J. Fiurasek and Z. Hradil, *Phys. Rev. A* **63**, 020101(R) (2001).
- [26] Y.-S. Kim, J.-C. Lee, O. Kwon, and Y.-H. Kim, *Nat. Phys.* **8**, 117 (2012).